TiO2 nanoparticles coated with bio-inspired ligands for the safer-by-design development of photocatalytic paints

Jérôme Laisney, Aurélie Rosset, Vincent Bartolomei, Daniela Predoi, Delphine Truffier-Boutry, Sébastien Artous, Virginie Berger, Grégory Brochard, Isabelle Michaud-Soret

TiO_2 nanoparticles coated with bio-inspired ligands for the Safer-by-Design development of photocatalytic paints

Jérôme Laisney,[a,†]* Aurélie Rosset,[a,b] Vincent Bartolomei,[b] Daniela Predoi,[c] Delphine Truffier-Boutry,[b] Sébastien Artous,[b] Virginie Bergé,[d] Gregory Brochard,[d] and Isabelle Michaud-Soret[a]*

Received 00th January 20xx,
Accepted 00th January 20xx

DOI: 10.1039/x0xx00000x

Addition of titanium dioxide nanoparticles (TiO_2 NPs) in photocatalytic paints represents a promising alternative aiming to mineralize gaseous pollutants, such as volatile organic compounds (VOCs). However, the risks of release of nanoparticles for human health and environmental impact have to be taken carefully into account for their development. To take in account these risks, we develop new way of TiO_2 NPs synthesis. Here, we report the electrostatic stabilization in aqueous media with pyrophosphate buffers of different pH range followed by the coating with bio-inspired molecules (lysine, deferoxamine, dopamine) and polymers (poly-acrylic acid, polyethylene glycol, poly-dopamine) of 4-5 nm spherical photocatalytic TiO_2 NPs for the development of safer-by-design photocatalytic paint. Characterization of the so-formed TiO_2 nanocomposites by dynamic light scattering (DLS), Fourrier-transformed infrared spectroscopy (FTIR), thermogravimetric analysis (TGA), scanning electron micrography (SEM), energy-dispersive X-ray spectroscopy (EDX) and X-ray photoelectron spectroscopy (XPS) showed the good grafting of the ligands on the TiO_2 surface and an enhanced stability in water compared to the pristine TiO_2 NPs. Photocatalytic activity of the TiO_2 nanocomposites was investigated by following the degradation of methylene blue (MB) under irradiation. Results showed a modulation of the photocatalytic activity (decrease or increase of the MB degradation rate) as function of the nature/binding strength of the bio-inspired coating on the oxide surface. Finally, the most promising nanocomposites were incorporated in paints on which preliminary chalking assays were performed after storage for one year in the dark or in interior daylight.

Introduction

Engineered nanomaterials (ENMs) and their outstanding surface properties, e.g. high surface/volume ratio, exalted surface reactivity, possibility of multi-functionality, have carried out great promises for a variety of industrial and consumers applications, making materials lighter, more robust and more efficient compared to their bulk analogues.[1] Since their emergence in the 1990's, nanotechnologies have already showed promises in revolutionizing the agriculture,[2] food,[3] textiles,[4] aerospace,[5] medicine,[6] or else energy[7] industries. Nowadays, more than 4330 nano-products are currently on the European market according to the nanodatabase,[8] with silver and TiO_2 among the most used ENMs.[9] As an example, the paint and coating industry is considering to introduce ENMs in their paint formulation to provide water repellence, scratch resistance, durability and antimicrobial properties to the paints.[10] In particular, rutile TiO_2 microparticles enters frequently in the paint formulation as pigment (whitener). The photocatalytic form (generally of anatase type) can adsorb UV-light and produce hydroxyl radicals in the presence of waters[11] leading to the degradation of organic molecules. The use of photocatalytically active TiO_2 under nanoparticulate size (TiO_2 NPs)[12] in paints was shown to degrade air contaminants such as NOx and VOCs in the presence of indoor light.[13] However, our recent study on such formulated paints[14, 15] have reported a degradation of the paint matrix (composed of binders, fillers, pigments and different additives like dispersing, thickeners and antifoam agents dispersed in water). This is due to the very strong photocatalytic activity of small TiO_2 NPs (4-5 nm in diameter) leading to the release of aerosolized particles as well as unwanted organic compounds from oxidized or partially oxidized VOCs (formaldehyde, methanol, acetaldehyde and formic acid) in the air during the use phase or mechanical solicitation. Consequently, there is a possible risk for workers and consumers to be exposed to NPs. This must be taken seriously into account in order to avoid serious health issues[16] such as encountered for asbestos. Thus, a safer-by-design approach[17] must be applied throughout the whole life cycle of self-cleaning paints (i.e. manufacture, use and end of life)[18] to minimize their environmental and toxicological impact. Furthermore, we showed previously that the particles release is sensitive to the paint formulation.[14]

In this context, we aim to apply a safer-by-design strategy relying on the chemical modification of the TiO_2 NPs used in the formulated self-cleaning paints of our previous study[15] (TiO_2 NPs referenced as P2) in order to: (i) modulate their photo-catalytic properties; (ii) improve their adhesion to the paint matrix and prevent their release, and (iii) reduce their toxicity. Many strategies such as defects introduction, chemical doping, noble metal deposition, dye sensitization or surface modification with ligands of different nature (organic/inorganic species, polymers) were developed in order to tune the photocatalytic properties.[19] This work only focuses on the coating of the TiO_2 NPs with a selection of bio-inspired ligands. A two-step protocol for embedding the TiO_2 NPs with the different coating

[a.] CEA – Grenoble, LCBM, Bioscience and Biotechnology Institute of Grenoble (BIG), UMR 5249 CEA/CNRS/UGA, 17, rue des Martyrs, 38000 Grenoble, France
[b.] Univ Grenoble Alpes, CEA, LITEN, DTNM, LMSE, F-38000 Grenoble, France.
[c.] National Institute of Materials Physics, Atomistilor 105 bis, Magurele 077125 Romania
[d.] ALLIOS, Les Docks II, 185 Chemin de Saint-Lambert, F-13821 La Penne-sur-Huveaune, France.
[†] Present address: Department of Plant and Soil Sciences, University of Kentucky, Lexington, KY 40546, USA.
*To whom correspondence should be addressed: jerome.laisney@gmail.com and isabelle.michaud-soret@cea.fr

was developed consisting in the electrostatic stabilization of the TiO_2 nanopowder in water by sonication in presence of an electrolyte that increase the electrostatic repulsive force. Then in a second step the addition of the ligand for coating the particles and provide a supplementary steric stabilization. The physico-chemical properties of the so-formed nanocomposites were investigated using various techniques (DLS, FTIR, TGA, XPS) as well as their photo-catalytic activity by following the degradation of methylene blue (MB) under light irradiation. The best nanocomposites will be selected according to specific criteria (photocatalytic performance, stability, affordability), then dispersed in paints to undergo chalking assays after storage for one year in the dark or in interior light conditions. The full characterization of the formulated paints is part of a separate publication.[20]

Materials and Methods

Chemicals

TiO_2 nanoparticles and chemicals.

CrystalActivPC500 anatase TiO_2 nanopowder (Tronox, Stamford, CT, USA), disodium pyrophosphate ($Na_2H_2P_2O_7$, purity ≥ 99%), tetrasodium pyrophosphate ($Na_4P_2O_7$, purity ≥ 95%), L-lysine (purity 98%), deferoxamine mesylate (purity > 92.5%), 3,4-dihydroxy-L-phenylalanine (purity > 98%), poly(acrylic acid) 3.5 kDa (PAA), polyethylene glycol of different molecular weight (10 kDa, 3350 Da, 200 Da referenced in the text as PEG10000, PEG3350 and PEG200), sodium nitrate ($NaNO_3$) and nitric acid were all purchased from Sigma Aldrich, USA. CellTak® was purchased from Corning (Corning, NY, USA).

TiO_2 nanoparticles coating

Electrostatic stabilization of TiO_2 NPs in aqueous media. (Step 1)

Optimal dispersion conditions were obtained for 2-10 mL aqueous suspension of TiO_2 NPs (10 $mg.L^{-1}$). These suspensions were sonicated for 1 h (pulse 1s on/off, 80% amplitude) in a cup-horn system (Vibracell 75041 ultrasonifier, Bioblock Scientific with a Sonics & Materials high intensity cup-horn), in presence of 5 mM of acidic ($Na_2H_2P_2O_7$, referenced in the text as H_2Pyro), neutral ($Na_2H_2P_2O_7$/$Na_4P_2O_7$ mix in a 1:1 v:v ratio) or alkaline ($Na_4P_2O_7$, referenced in the text as NaPyro) pyrophosphate buffer.

Embedding and steric stabilization of TiO_2 NPs with the bio-inspired coatings. (Step 2)

Ligand solutions were introduced dropwise into the TiO_2 NPs suspension previously stabilized. The solutions were prepared with optimal conditions of concentration and pH, concentration of ligand (C_L) and volume added (Ti_{surf}/ligand stoichiometric ratio of 1/1) to trigger an exchange ligand reaction between the hydroxylated surface and the ligands (Table S1). The concentration of titanium on surface sites (Ti_{surf}) was determined according to the Equation 1. [21]

$$[Ti]_{surf}=[TiO_2].12.5/D \quad (1)$$

Where $[TiO_2]$ represents the molar concentration ($mol.L^{-1}$) of TiO_2, and D, the particle diameter in Ångstrom. We estimated a concentration of Ti_{surf} of 39 mM taking into consideration a primary particle size of 4 nm and a concentration of 10 $mg.mL^{-1}$. The pH was also adjusted in order to fully protonate (PAA) or deprotonate (lysine, deferoxamine, Dopa, PEGs) the ligand for an optimal reactivity with the negatively or positively charged TiO_2 surface. The mixture was then stirred at 60 °C for 1 h in an Omni station OS1025 reactor (Electrothermal, Fisher Scientific, Waltam, MA, USA) allowing homogeneous heating of the solution. The particles were collected by centrifugation at maximum speed for 10 min, washed three times with water to remove unreacted ligand and dried overnight at 50 °C in an oven. The particles were then stored in the dark at 4 °C.

Characterization

Scanning electron microscopy (SEM).

The size and morphology of TiO_2 NPs were investigated by ultra-High Resolution Scanning Electron Microscopy (HR-SEM, LEO 1530, Germany). Images were acquired with a working distance of 3.6 mm, an accelerating voltage of 5kV, a magnification of x 100 K and a diagram aperture of 30 µm. The elementary chemical composition of TiO_2 NPs was analyzed by Energy Dispersive X-ray spectrum (EDX, QUANTAS EDS, Bruker Nano assisted software ESPRIT, USA) in the SEM. The working distance and accelerating voltage were respectively raised to 8 mm and 15kV.

Dynamic light scattering (DLS).

The hydrodynamic radius of the nanoparticles (averaged in % intensity or % mass) and polydispersity were measured by DLS using a DynaPro NanoStar from Wyatt Technology (Santa Barbara, CA, USA). The suspensions of NPs were diluted in ultrapure water at a concentration of 100 $\mu g.mL^{-1}$ and filtered on a 0.45 µm membrane prior to measurement to get rid of non-dispersible aggregates.

Zeta potential.

Surface charge was evaluated by electrophoretic mobility using a Zetasizer Nano ZSP (Malvern Instruments, Worcestershire, UK). 50 $\mu g.mL^{-1}$ of TiO_2 NPs were sonicated for 5 min in 13 mL of deionized water and 10 mM of sodium nitrate ($NaNO_3$). Electrophoretic mobility was measured from low pH by adding small amount of nitric acid HNO_3 to adjust the pH.

Fourrier-transformed infrared (FTIR) spectroscopy.

The presence of the coating on the TiO_2 surface was verified by FTIR. FTIR spectra were recorded at RT on transmission mode (scan resolution: 4 cm^{-1}) with 1 mg of dried powders pelleted with 99 mg of KBr and using a Spectrum 100 PerkinElmer spectrometer (PerkinElmer, Waltham, MA. USA).

Thermogravimetric analysis (TGA).

Quantification of the coating surrounding the TiO_2 NPs was measured by TGA using a SDT Q600 from TA instruments (Water Corporation, Milford, MA, USA). The samples followed up a heat cycle between 20 and 800 °C at a heating rate of 10°C/min. The weight derivative as a function of the temperature (dashed curves) was represented along with the weight variation for a

finer analysis of the weight fluctuation over the temperature range.

X-ray photoelectron spectroscopy (XPS) analysis.
The grafting mode was determined by XPS using a 1486.61 eV Al Kα monochromatic X-ray source (SPECS GmbH, Berlin, Germany). Survey (0 - 1400 cm^{-1}) and high-resolution (C1s, Ti2p and O1s) spectra were recorded. The atomic percentage of each element was determined from the high-resolution spectra using Spectral Data Processor software. The binding energy of spectra was calibrated from carbon C1s peak at 285 eV corresponding to the hydrocarbon (C-C/C-H).

Photocatalytic activity.
The photo-catalytic activities of the nanocomposites were measured with MB as a target molecule under UV-Vis irradiation. The degradation of MB in presence of TiO_2 NPs was followed according to the evolution of the absorbance at 655 nm measured by UV-visible spectroscopy (Cary 100, Agilent technologies, Santa Clara, CA, USA). The experimental setup consists of a Xe source (P = 300 W, λ > 300 nm) (Newport, MKS Instruments Inc., Andover, MA, USA) equipped with a liquid filter filtering wavelengths greater than 800 nm to prevent heating and evaporation of the solution. 10 $mg{\cdot}mL^{-1}$ of TiO_2 NPs suspensions in water or in 5 mM NaPyro were prepared by weighing a mass of TiO_2 accordingly to the TGA results for TiO_2 concentration in each sample then sonicated for 1 h (pulse 1s on/off, 80% amplitude) in a cup-horn system. The TiO_2 suspension was then diluted in 2 mL of a 12.5 $\mu g{\cdot}mL^{-1}$ aqueous solution of MB to reach TiO_2 NPs concentrations ranging between 0-100 $\mu g{\cdot}mL^{-1}$. The solution was then placed in a quartz cuvette and irradiated under stirring at a power between 2.1 and 2.2 suns (210 and 220 $mW{\cdot}cm^{-2}$). UV-vis spectrum in the 200-800 nm range was recorded at different time points over a period of 2 h.

Paint formulation and chalking assay.
Photocatalytic paints were formulated with TiO_2 NPs and TiO_2 NPs coated with Dopa, PEG3350 and PAA. Slurries of TiO_2 nanopowders with a TiO_2 concentration of 35 wt% were prepared in 5 mM neutral pyrophosphate buffer to ensure optimal dispersion conditions. The particles were then incorporated in the paint as described in ref [20] with a final TiO_2 NP content of 3.5 wt%. The formulated paints were then applied on a Leneta substrate using a manual film applicator with a wet thickness of 150 µm. The paints were then stored at room temperature for one year in the dark or under interior day light before undergoing a chalking assay according to the NF EN ISO norm 4628-3. Experimentally, the chalking resulting from ageing was removed with a tape then examined on a contrasting background. The degree of chalking was evaluated using a reference scale quotation.

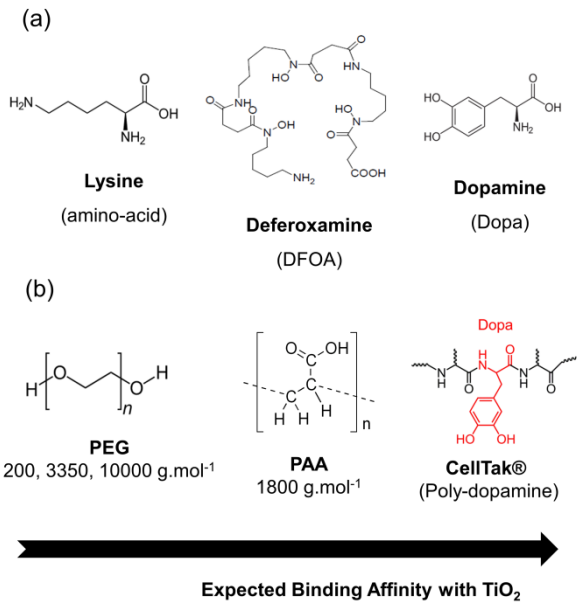

Fig. 1: Selected bio-inspired molecules (a) and polymers (b) and their expected binding affinity with the TiO_2 NPs surface.

Results and discussion

1. Electro-steric stabilization of photocatalytic TiO_2 NPs with bio-inspired ligands

Selection of bio-inspired ligands.

The selected bio-inspired coatings are presented in Fig. 1. They were chosen according to specific criteria such as biocompatibility, adhesion properties and hydrophilicity to reduce the toxicity of the particles, adhere to the paint matrix *via* supplementary bonds and work under mild conditions such as in aqueous medium. They also possess different binding mechanism (covalent *versus* non-covalent) and functional groups to vary the binding strength on the TiO_2 surface. These coatings can be divided into two categories: (a) low molecular weight natural ligands and (b) bio-compatible polymers. Among the molecular coatings (Fig. 1a) were selected the lysine amino-acid, the deferoxamine siderophore (DFOA) and the dopamine (Dopa) molecule, well known for its ability to bind iron and TiO_2 films via the catechol functional group.[22] Since these coatings possess an affinity with Fe(III), we expect these molecules to bind covalently via a coordination bond to the Ti(IV) sites on the surface of the particles. For the bio-polymers category (Fig. 1b), polyethylene glycol (PEG) and polyacrylic acid (PAA) were chosen due to their regular use in the synthesis of nanoparticles conferring them stabilization, biocompatibility and bio-adhesion properties. [23-29] In contrast to the previous class of coatings, these polymers bind to the surface via a multiplicity of weaker interactions such as hydrogen bonds or van der Waals contacts. Different molecular weights of PEG were selected (M_W = 200, 3350, 10000 $g.mol^{-1}$) to vary the thickness of the coating layer around the TiO_2 surface. Finally, we chose a derivative of Mfp (Mussel Foot Protein) type proteins that possess considerable adhesion properties on any kinds of surfaces (dry

or wet) related to the presence of Dopa and lysine within the protein chain.[30-32] In particular, CellTak® is a commercial poly-dopamine Mfp protein used for cells adhesion on substrates and containing 5% Dopa formed by the repetition of the decapeptide (Ala-Lys-Pro-Ser-Tyr-Hyp-Hyp-Thr-Dopa-Lys)$_x$ (x = 80 - 100).[33]

Electrostatic stabilization of the TiO_2 NPs with an electrolyte.

SEM image and EDX spectrum of the TiO_2 NPs, presented in Fig. S1, showed the presence of large clusters of a few microns composed of spherical NPs with a diameter of approximately 4-5 nm, as already reported in our previous study.[15] For a uniform and efficient coating around the NPs, an effective method is needed first to break the clustering of particles[34] then to stabilize the suspension in aqueous medium for allowing the ligand to interact with the oxide surface. Pyrophosphates have proven to be an effective electrolyte for the dispersion of TiO_2 nanopowder.[33] The acidic ($Na_2H_2P_2O_7$, pH 4.5) and alkaline forms ($Na_4P_2O_7$, pH 8.5) of pyrophosphate, designed respectively as H_2Pyro and NaPyro, open the possibility for two synthetic routes according to the physico-chemical properties of the bio-inspired ligands (e.g. acceptor or electron donor, pH of the ligand in aqueous solution). The zeta potential of the particles measured as a function of the pH (Fig. S2) gives an estimation of the point of zero charge of the TiO_2 NPs in water located around pH 5.0. Based on this result, dispersion in H_2Pyro will protonate the water layer on the particle surfaces and lead to a positively charged TiO_2 surface (ξ = +5-10 mV) while the basic pyrophosphate form will lead to the reduction of the surface water layer with the presence of hydroxyl ions and negative charges (ξ = -35 mV). Contrary to pure dispersions in water leading to a rapid sedimentation of the powder, the suspensions in presence of pyrophosphate remains stable. DLS measurements performed on the suspensions (Fig. 2) shows the different particle sizes population in mass-weighted average. After sonication, two populations were observed for both conditions. A population predominant in mass (main peak) of small particles with a hydrodynamic radius measured in the 3-5 nm range, i.e. compatible with the size of the primary particles (2-2.5 nm radius), and clusters of a hundred of nanometers. In addition to the good dispersion in the particle size (PDI of the main peaks < 0.05), the colloidal solutions are stable from several hours to several days with a slightly improved stability when the particles were sonicated in presence of the basic pyrophosphate form. The improved stability of the particles can be easily explained by the value of the zeta potential of the particles with a higher global surface charge at pH 8.5 compared to pH 4.5 providing higher repulsive electrostatic forces. Indeed, according to the Derjaguin-Landau-Vervey-Overbeek (DLVO) theory,[35] the aggregation or dispersion of particles in solution is governed by the relative intensity of two main forces: (i) attractive force of van der Waals and (ii) repulsive electrostatic force. In an aqueous medium, the low overall charge of the nanoparticles surrounded only by water molecule does not provide enough repulsive force to avoid the rapid aggregation of the particles in solution.

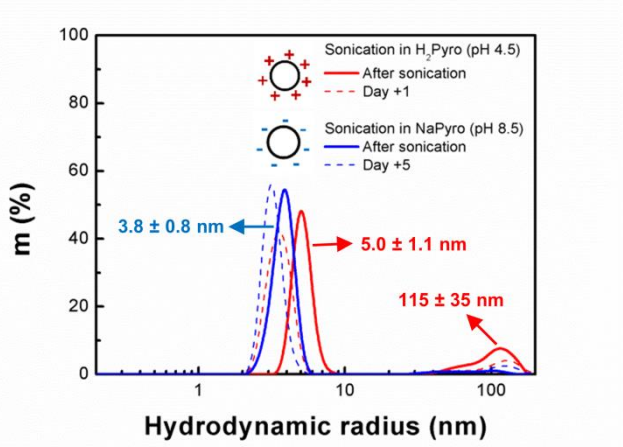

Fig.2: Hydrodynamic radius measured by DLS (mass-weighted average) of an aqueous suspension of TiO_2 NPs sonicated in presence of 5 mM pyrophosphate in acid (H_2Pyro, pH = 4.5) or basic form (NaPyro, pH = 8.5). Measurements performed after sonication (—) and before aggregation (- - -).

Coating of TiO_2 NPs with the bio-inspired ligands.

After dispersion and stabilization in presence of pyrophosphate, a solution of ligand was added dropwise to the TiO_2 NPs suspension with optimized ligand concentration C_L and pH (Table S1). As an example, PAA has a pKa of 4.5 meaning that the functional groups of the acrylic acid monomer are undissociated and positively charged below 4.5.[36] As the pH of a PAA solution at C_L is 2, the TiO_2 NPs were then sonicated in presence of the basic form of pyrophosphate to provide negative charges to the surface and trigger an electrostatic reaction between the TiO_2 NPs and the polymer. Concerning the reaction of Dopa on the TiO_2 surface, it is reported in the literature[37] that Dopa binds the Ti(IV) sites according to two coordination modes depending of the pH. The first one so-called salicylate mode at acidic pH in which the protonated or partially protonated Dopa binds the Ti(IV) via hydrogen bonds. The second one, a catecholate mode (pH > 7) in which the binding involved two coordination bonds from the two deprotonated oxygens. The catecholate binding mode on the photocatalytic properties was only investigated by preparing the Dopa in basic medium (deprotonated form). In the particular case of the CellTak® coating, the attachment on the surface is achieved after the sudden raise of the pH from neutral to basic.

After reaction, the nanocomposites powders involving the covalent grafting (biomolecules and CellTak® coatings) exhibits different color from pale yellow to dark brown compared to the original bright white TiO_2 NPs powder and the non-covalent grafting composites (PEG and PAA). These different optical properties can be an indicator of the good grafting of the molecules on the surface as covalent grafting involves coordination bonds creating charge transfer bands (Ligand-to-Metal type) in the visible domain or the polarization of the dipole moment.[38] The evolution of the NPs size after addition of the bio-inspired ligands was followed by DLS (Fig. S3). After addition of the bio-inspired ligands and ageing in the dark, the population of the particles progressively evolved over time toward clusters of a hundred of nanometers before their aggregation. From this dataset, we estimated the stability of the

different suspensions after their electro-steric stabilization (Table 1). It is worth noticing that the stability of the NPs was improved when coated with the different bio-inspired ligands compared to TiO_2 NPs suspended in water and pyrophosphate. The particles coated with Dopa, PEG3350 and PAA present the best stability with a lifetime in the dark superior to 6 months. However, the particles coated with Lysine, PEG200, and PEG10000 aggregates after only one month. In the case of particles coated with CellTak®, the addition of ligand causes the formation of large size assemblies that rapidly settles down. After reaction, the nanocomposites were collected by centrifugation for further characterization.

Table 1: Stability and photo-catalytic properties of the TiO_2 nanocomposites as a function of the dispersing medium and the bio-inspired coatings.

Coating	Electrolyte	Stability$^{\Phi}$	$t_{1/2}$ (min) (50 µg.mL^{-1})$^{\Psi}$	Photo-catalytic activity $^{\zeta}$ (%)
-	-	A few minutes	27.3	-
-	H_2Pyro	A few hours	-	-
-	NaPyro	A few days	-	-
Lysine	H_2Pyro	2 weeks	34.2	-25
DFOA	H_2Pyro	1 month	45.8	-68
Dopa	NaPyro	> 6 months	85.6	-214
PEG200	H_2Pyro	1 month	33.1	-21
PEG3350	H_2Pyro	> 6 months	48.8	-78
PEG10000	H_2Pyro	1 month	36.4	-33
PAA	NaPyro	> 6 months	22.2	+18
CellTak®	Pyro neutral buffer	Aggregation	67.8	-148

(ϕ) Qualitative estimation according to DLS measurements (Fig. S3) of the electro-steric stabilized TiO_2 NPs suspensions sonicated in pyrophosphate buffer and coated with the different bio-inspired ligands. (ψ) Half-degradation time of MB under UV-vis irradiation with the TiO_2 nanocomposites. (ζ) Decrease (-) or increase (+) of the photocatalytic activity (PA) of the TiO_2 nanocomposites was determined from $T_{1/2}$ (MB) of the composites compared to $T_{1/2}$ (MB) of the pristine TiO_2 NPs according to the formula PA=($T_{1/2}$ composite -$T_{1/2}$ pristine TiO_2 NPs).100/ $T_{1/2}$ pristine TiO_2 NPs.

2. Characterization of the TiO_2 nanocomposites

Grafting of the ligands by FTIR spectroscopy.

FTIR spectra of the powders were collected to verify the good grafting of the bio-inspired ligands on the surface. Fig. 3 shows the FTIR spectra in the 1850-1000 cm^{-1} range for the pristine TiO_2 NPs and the so-formed nanocomposites after ligands addition. In this range, characteristics bands attributed to the TiO_2 NPs can be found at 1630 cm^{-1} and 1114 cm^{-1} corresponding to the Ti (TiO_2)-O (H_2O) and O (TiO_2)-O (H_2O) vibrations between the titanium or oxygen from the TiO_2 surface and the oxygen from the hydroxyl layer. According to the literature,[39] the characteristics vibration band of TiO_2 observed at 1400 cm^{-1} can be attributed to the vibration of Ti-O bonds inside the TiO_2 crystal lattice. Other characteristic vibrations of TiO_2 outside this range can be found at 660 cm^{-1} (vTi-O-Ti) and between 3700 and 2600 cm^{-1}, attributed to the hydrogens vibration from the hydroxyl layer (Fig. S4 for the full range FTIR spectra). In addition to the characteristic vibrational bands of TiO_2, additional bands are visible in the spectra of the nanocomposites. A clear additional band appears in the TiO_2-PAA nanocomposite spectrum (Fig. 3e) that can be attributed to the C=O from the carboxylate functional group of the acrylic acid monomer. Similarly, the TiO_2-PEG nanocomposite spectrum (Fig. 3d) presents an intense band at 1106 cm^{-1} that could be due to the O-O vibration band between the PEG polymeric chains and the O from the TiO_2 surface or the hydroxyl layer. The TiO_2-Dopa (Fig. 3c) and other bio-molecular coatings (Lysine, Fig. 3a; DFOA, Fig. 3b) lets appear additional vibration bands at 1490 cm^{-1} and 1270 cm^{-1} that can be attributed to the vibrations of C-NH_2 and C-O functional groups present in these ligands. The assignment of the bands for the other coatings can be found in Table S2. As those additional bands are characteristic of functional groups and chemical bonds present in the different ligands, FTIR characterization could indicate their good grafting on the surface.

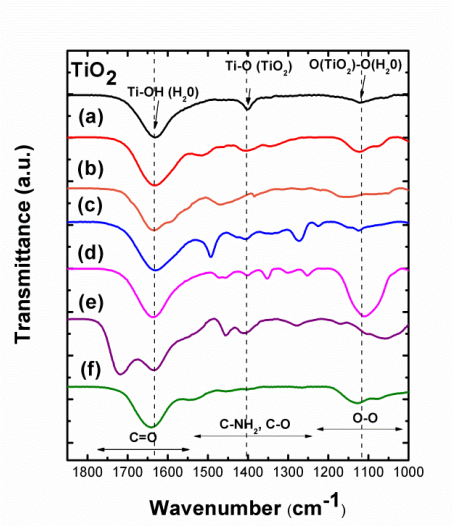

Fig. 3: FTIR spectra (KBr pellet) in the 1850-1000 cm^{-1} of the TiO_2 NPs (in black) and TiO_2 NPs coated with (a) Lysine, (b) Deferoxamine (DFOA), (c) Dopa (catecholate), (d) PEG3350, (e) PAA and (f) CellTak®. The spectra were normalized according to the peak at 1630 cm^{-1} ($\nu_{Ti\text{-}OH}$).

Quantification of the coating by thermogravimetric analysis (TGA).

To confirm and quantify the coating around the TiO_2 NPs surface, thermogravimetric analysis (TGA) was performed on the nanocomposites (bio-molecules, Fig. 4a and bio-polymers, Fig. 4b). In the thermograms were observed several weight losses associated to the departure of chemical species during the thermal cycle. A first weight loss associated to the dehydration of the samples (T_{water}<100 °C) was observed for all the nanocomposites. After dehydration, a weak weight loss was observed soon after (T = 172.6 °C) for the pristine TiO_2 NPs that could potentially be associated to the impurities surrounding the NPs surface. Additional weight losses were observed in the thermograms of nanocomposites at a temperature relatively close to the temperature observed in the case of the departure of the free bio-inspired ligands (Fig. S5) allowing us to unambiguously confirm the good grafting of the ligands on the surface. At 800 °C, all the different organic coatings were sublimated and the remaining product/weight was associated to TiO_2. All the different features that can be extracted from the thermograms are presented in Table 2. The nanopowders contain between 6 and 12 wt% of water depending on the drying as the departure of water occurs below 50 °C for most of them. The weight content of TiO_2 in the different samples, including the initial nanopowder, is found below 85 wt%.

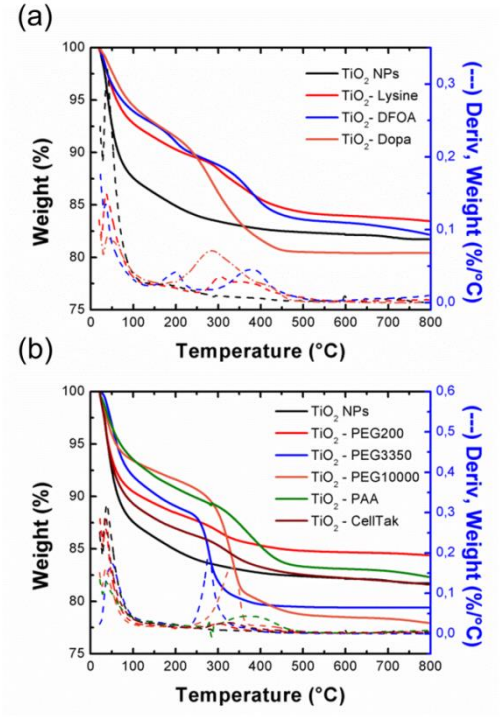

Fig. 4: Thermograms of the TiO_2 NPs (in black) and TiO_2 NPs coated with the different bio-inspired molecules (a) and polymers (b). Dash curve: derivative function of the weight as a function of the temperature.

Table 2: Dehydration temperature (T_{water}), thermal decomposition of the ligand (T_{Ligand}), decomposition temperature of the ligand coated on the TiO_2 surface ($T_{coating}$), and global composition of the TiO_2 nanocomposites (water, coating and TiO_2 contents) extracted from the thermograms.

Sites	T_{water} (°C)	T_{Ligand} (°C)	$T_{coating}$ (°C)	Water content (wt%)	Coating content (wt%)	TiO_2 content (wt%)
TiO_2	37.9	N.A.	-	12	-	82
TiO_2–Lysine	35.5	N.A.	303.1	8	5	83.5
TiO_2–DFOA	35.1	208.0 387.6	200.9 377.3	6.5	6-7	82
TiO_2–Dopa	38.7	280.1 501.6	280.2 405.6	10	2.5	81.5
TiO_2-PEG200	36.2	215.8	307.4	10	2	84
TiO_2-PEG3350	80.0	256.4	277.0	6	17	76
TiO_2-PEG10000	36.6	251.3	333.9	7	10	78
TiO_2–PAA	36.8	246.0 315.4 505.6	378.1	7	6-7	82
TiO_2–CellTak	36.8	N.A.	323.6	11.5	3	82

N.A.: not available

Adsorption mode and thickness of the coating by X-ray photo-electron spectroscopy (XPS).

The TiO_2 nanocomposites were analyzed with XPS to determine the grafting mode of the bio-inspired ligands on the TiO_2 surface. The high-resolution XPS spectra of C1S, Ti2p and O1s region of the pristine and coated TiO_2 NPs are represented in Fig. 5. The carbon C1s peak was composed of three peaks at 284.82 ± 0.04 eV, 286.1 ± 0.45 eV and 289.15 ± 0.45 eV binding energies. The first peak was associated to C-C or C-H bonds.[40, 41] The peaks at 286.1 ± 0.45 eV and 289.15 ± 0.45 eV were attributed respectively to C-O and O=C-O bonds.[40] For the TiO_2 -PEG3350 nanocomposite, the peak at 289.15 ± 0.45 eV is not present. For the TiO_2-Dopa, TiO_2-PEG3350, TiO_2-PAA and TiO_2-DFOA nanocomposites, a supplementary peak appeared at 287.76 ± 0.24 eV. This peak was attributed to C=O bonds.[40] On the other hand, previous studies[42, 43] have shown that the peaks at 287.76 eV and 289.15 eV may be from atmospheric contamination. The both peaks at 286.1 ± 0.45 eV and 287.76 ± 0.24 eV can be originated from the ligands. In the case of pristine TiO_2 NPs, C-O bonds could come from a carbon layer surrounding the particles.[15] The peak at 288.76 eV was only observed for the TiO_2-PAA nanocomposite and assigned to –O-C=O bonds.[44-46] The titanium Ti2p peak was composed of two main peaks assigned to Ti $2p_{3/2}$ and Ti $2p_{1/2}$ core levels of Ti^{4+} at 458.97 ± 0.09 eV and 464.63 ± 0.17 eV, respectively.[47, 48] The predominant peak at 458.97 ± 0.09 eV was attributed to Ti^{4+} ions in TiO_2.[48, 49] This indicates that these ions are in an octahedral environment, coordinated with oxygen.[50, 51] XPS spectrum of TiO_2-Dopa and TiO_2-DFOA nanocomposites show that the Ti $2p_{3/2}$ and Ti $2p_{1/2}$ was shifted toward a lower binding energies compared to pristine TiO_2 NPs, approximatively of 0.21 eV and 0.36 eV, respectively. This confirms that the bond between TiO_2 and Dopa and DFOA is based on C-O-Ti and not C-Ti.[52] For the TiO_2-Dopa nanocomposite, two supplementary peaks appeared at 460.46 eV and 466.04 eV, which belong to the N-Ti-O bonds and C-O-Ti, respectively.[53] This C-O-Ti binding in titanium Ti2p compared to pristine TiO_2 NPs was attributed to covalent interaction of the ligand with Ti sites at the surface. The new peak in titanium Ti2p corresponding to N-Ti-O suggest an electrostatic interaction between the positively charged NH_3^+ groups in the ligands with O^{2-} sites at the surface. The grafting of Dopa on the TiO_2 NPs surface could be the result of a combination of covalent interaction (C-O-Ti bonds) and electrostatic interaction via protonated NH_2 at the surface whereas the grafting of DFOA on the TiO_2 NPs surface is purely covalent. The binding energies are now 457.48 eV and 462.92 eV were attributed to Ti $2p_{3/2}$ and Ti $2p_{1/2}$ of Ti^{3+}.[54, 55] This means that the Ti^{3+} sites were created in nanocomposites during the grafting. This oxidation of Ti sites at the surface could be due to absorption of the DFOA on the TiO_2 surface. The deconvolution of the O1s spectrum shows a main peak at 530.30 ± 0.13 eV attributed to oxygen atoms of TiO_2 lattice and various minor peaks at higher binding energies.[56] The minor peaks at 531.33 ± 0.04 eV and 533.09 ± 0.09 eV were assigned respectively to OH and H_2O species, indicating the presence of hydrated oxides at the TiO_2 surface.[57] For the TiO_2-PEG3350 and TiO_2-PAA nanocomposites, new bonds appeared compared to XPS spectra of pristine TiO_2 NPs. A slight shift of the peak at 531.33 ± 0.04 eV is observed for TiO_2-PEG3350 and TiO_2-PAA nanocomposites, of approximately 0.25 eV, probably due to the adhesion of the ligands. The peak at 533.09 ± 0.09 eV was not observed for the pristine TiO_2 NPs and TiO_2-PAA nanocomposite. However, for pristine TiO_2 NPs, a peak at 532.47 eV appears. This peak can be assigned to C-O bonds[52] which comes from a carbon layer coating surrounding the particles. B.F. Xin et al.[58] suggest that the peaks at binding energy at 531-533 eV can be attributed to oxygen chemisorbed such as O_2, -OH, and $-CO_3$ on TiO_2 surfaces. Moreover, the peak at binding energy at 533.87 eV can be assigned to the oxygen atoms connected to carbon atoms in C-O.[59] This suggests that the grafting with the polymers is a non-covalent grafting occurring preferentially on O sites at the TiO_2 surface. The concentration of each elements related to the nanocomposites were also determined by XPS. Table S2 presents the average chemical composition measured over each sample. The pristine TiO_2 NPs contain 8.30 at% of carbon, which is coming from a thin carbon layer contamination surrounding the particles. This result is in agreement to thermogravimetric measurements. For the TiO_2-Dopa, TiO_2-PEG3350, TiO_2-PAA and TiO_2-DFOA nanocomposites, the carbon concentration is about 2.6 times higher than for pristine TiO_2 NPs. This indicates that the carbon finds its origins from the ligands. Elements such as F, N, P and Na were also present in our spectra and represent a total of 3 at%.

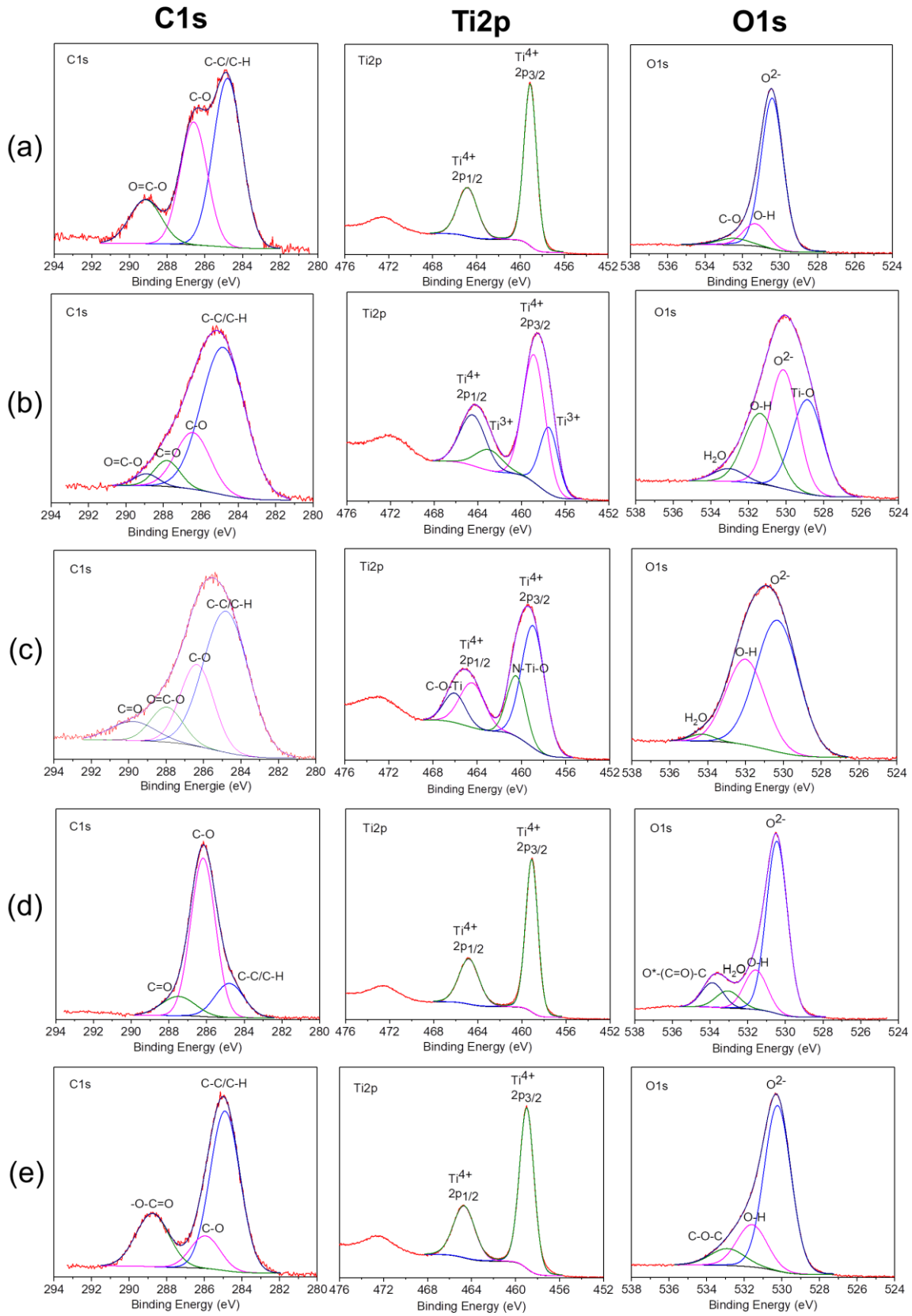

Fig. 5: XPS spectra of pristine TiO_2 NPs and TiO_2 NPs coated with bio-inspired ligand. C1s, Ti2p and O1s spectra of (a) pristine TiO_2 NPs, TiO_2 NPs coated with (b) deferoxamine (DFOA), (c) Dopa, (d) PEG3350 and (e) PAA.

Coating rate of the TiO_2 NPs.

Taking into account the molar amount of active sites available (O and/or Ti) deduced from Jankovic et al.[60] formula for an anatase spherical particles (Text S1), the grafting mode on the surface from the XPS study (covalently and/or electrostatically via Ti and/or O sites, respectively), the denticity of the ligand and the amount of coating present on the surface extracted from TGA, one can estimate the particle coating rate for the different ligands (Table 3). Variability among the nanocomposites was observed depending on the chemical nature of the ligand (molecular weight, grafting mode, denticity) and its affinity with the TiO_2 surface. The highest coating rate in the case of bio-molecules and polymers was found respectively with Dopa (24.3% of active sites coated) and PEG10000 (coated surface of approximately 42.6%). Among the molecular coatings, Dopa has a highest binding affinity with the TiO_2 surface than Lysine (12.56%) and DFOA (5.25%). The covalent grafting mechanism offers a fewest available sites for the adhesion of the ligand (reaction with the titanium sites only) compared to non-covalent grafting (multiple van der Waals-type interactions with the Ti and O sites but also hydrogens bonding with the hydroxyl layer). However, this estimation takes only into account the ideal case where the nanoparticles are perfectly dispersed in solution (primary TiO_2 NPs with a diameter of 4 nm). Indeed, DLS measurements of the nanocomposites (Fig. S3) rather indicated the presence of clusters of particles of a 100 nm radius decreasing drastically the number of available surface sites for the adsorption/exchange reaction with hydroxyl groups to take place.

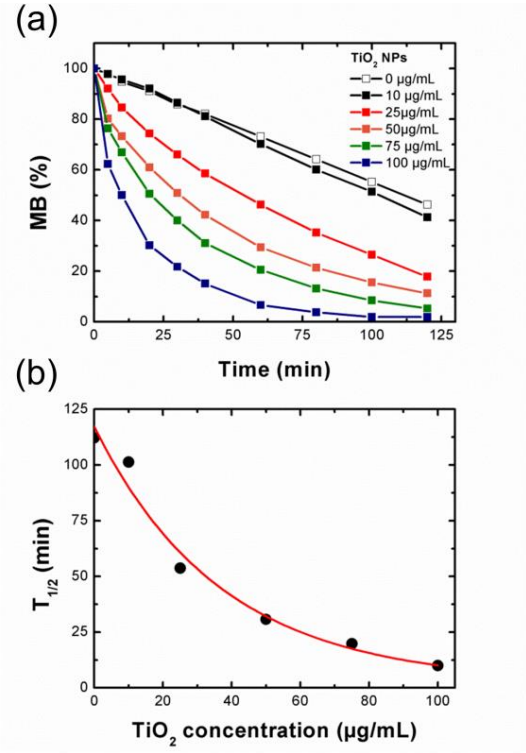

Fig. 6: Photocatalytic activity of the TiO_2 NPs in water (pH 7.0). (a) Degradation of MB under UV-vis irradiation as a function of the TiO_2 NPs concentration. (b) Half-degradation time of MB (time necessary to deteriorate 50% of MB) as a function of the TiO_2 NPs concentration. MB (%) = $((A_{665nm,\,t} - A_{665nm,t0})/A_{665nm,t0})x100$.

Table 3: Composition of the TiO_2 nanocomposites (water, TiO_2, coating) for 100 mg of powder according to TGA and estimation of the coating rate of one particle.

Nanocomposite	M_{ligand} ($g.mol^{-1}$)	n denticity	H_2O (mg)	TiO_2 (mg)	Coating (mg)	TiO_2 adsorption sites[α]	Coating (theory) (mg)[β]	Coating rate (%)[γ]
TiO_2-Lysine	146	1	10.5	83.5	6.0	Ti	47.8	12.6
TiO_2-DFOA	656.8	1	6.6	82.3	11.1	Ti	211.5	5.2
TiO_2-Dopa	197.2	1	4.4	80.5	15.1	Ti	62.1	24.3
TiO_2-PEG200	200	4	12.0	84.4	3.6	O	33.0	10.9
TiO_2-PEG3350	3350	60	10.9	79.4	9.7	O	34.7	28.0
TiO_2-PEG10000	10000	178	7.4	78.0	14.6	O	34.3	42.6
TiO_2-PAA	1800	25	9.7	82.4	7.9	O	46.4	17.0
					7.9	Ti+O	69.6	11.3
TiO_2-CellTak	140000	1000	13.1	81.7	5.2	Ti	44.8	11.6

[α] preferential TiO_2 adsorption site based on XPS investigation, [β] theoretical mass of ligand necessary to bind the entire active sites of a 4 nm spherical anatase particle, [γ] coating rate (CR) calculated according to the formula CR = (experimental coating mass/theoretical coating mass)*100.

3. Photocatalytic activity

Degradation of Methylene Blue (MB) as a function of the TiO_2 NPs concentration.

The photocatalytic activities of the TiO_2 nanocomposites were evaluated by following the degradation of MB under UV-vis irradiation. The emission spectrum of the lamp can be found in Fig. S6. TiO_2 is a wide-bandgap semi-conductor with 3.0-3.2 eV of bandgap energy (Eg) that requires the light excitation with a wavelength range shorter than 400 nm. The photogeneration of electron-hole pairs and reactive radicals ($HO^{\bullet}$, $O_2^{\bullet-}$) participates in reduction and oxidation processes at the surface. A first set

of experiment was conducted by looking at the degradation of MB as a function of the TiO_2 NPs concentration (Fig. 6 and Fig. S7). Fig. 6a presents the degradation of MB as a function of TiO_2 concentration (0-100 µg.mL^{-1}). The results show a linear degradation of MB under irradiation in the absence of TiO_2 with 46% of the MB degraded after 2 h of irradiation. However, a faster degradation is clearly observed when MB is irradiated in presence of the TiO_2 NPs. This photolysis is considerably accelerated when increasing the TiO_2 NPs concentration. Fig. 6b represents the half-degradation time of MB ($t_{1/2}$, time necessary for degrading 50% of MB under irradiation) as a function of the TiO_2 NPs concentration. The recorded points fit well with an exponential fitting. Therefore, 50% of the MB is completely degraded after 100 min of irradiation at a concentration of 10 µg.mL^{-1}. This time decrease down to 10 min at a concentration of 100 µg.mL^{-1}.

Influence of the coating on the photo-catalytic activity.

This first series of experiments showed that the photocatalytic activity is highly sensitive to the TiO_2 concentration. For the following experiments, we fixed a TiO_2 NPs concentration of 50 µg.mL^{-1} in order to observe fine changes in the photocatalytic activities. To make sure to get the same TiO_2 amount in every sample and compare the photo-catalytic activity of the different nanocomposites, the mass necessary to prepare the 50 µg.mL^{-1} solutions was weighted according to the TiO_2 wt% content found by TGA. Because the photocatalytic activity is strongly influenced by the pH,[61] the activities of TiO_2 NPs coated with bio-inspired ligands (Fig. 7) were evaluated at pH 7.0. Fig. 7a and Fig. 7b show the degradation of MB under UV-vis irradiation in presence of the nanocomposites in the case of the bio-molecular and bio-polymeric coatings, respectively (Fig. S8). The superimposition for all coatings can be found in Fig. S9 and the photocatalytic activity ($T_{1/2}$) compared to the pristine TiO_2 NPs is reported in Table 1. The dataset nicely shows a good modulation of the photo-catalytic activity with the different coatings surrounding the TiO_2 NPs. For the bio-molecule coatings (Fig. 7a), the photo-catalytic activity is slightly reduced with Lysine and DFOA coatings. However, the photo-catalytic activity is strongly decreased when the TiO_2 NPs are coated with Dopa that possesses a stronger binding affinity toward the TiO_2 surface and a higher coating rate compared to Lysine and DFOA. Two regimes can clearly be observed: a slow degradation of MB between 0 and 40 min followed by a more rapid degradation with a progressive increase of the standard deviations. This suggests a deterioration of the Dopa coating over time as its photodegradation by TiO_2 have already been observed in aqueous media.[62] In the case of bio-polymers (Fig. 7b), the coating of the TiO_2 NPs with PEG of different molecular weights shows different behaviors. The photocatalytic activity is less impacted with PEG200 (-21%) and PEG10000 (-33%) contrary to PEG3350 coating where a decrease of the activity by around -80% was found. PEG200, PEG3350 and PEG1000 have an increasing coating rate according to the TGA calculations (Table 3), which can be directly correlated to the thickness of the polymeric layer on the surface. Based on these results, we can assume that the photocatalytic activity is influenced by the thickness of the polymeric layer coating, but further investigations are needed to ascertain this hypothesis. A strong decrease was also observed for the CellTak® poly-dopamine with possible deterioration of the coating as the same behavior than Dopa can be noticed (two distinct regimes with a more intense degradation and progressive increase of the standard deviation over time). Contrary to Dopa and the polyDopa, PEG3350 coating seems to be more stable over the irradiation cycle. Interestingly, the TiO_2-PAA nanocomposite is the only coating exhibiting an increase of the photocatalytic activity by around 20%.

The photocatalytic activity seems very sensitive to a change at the surface of the TiO_2 nanoparticles. It was shown that the activity depends on both intrinsic TiO_2 NPs properties (crystallinity, surface charge, particle size, presence of defect sites) and interfacial interactions with the substrate.[63] As the intrinsic TiO2 NP properties and experimental conditions (pH, concentration) were kept identical in the different experiments, the decrease can be explained by a less surface available for the adsorption/degradation reaction of MB to take place because of the surface coverage by the ligand.

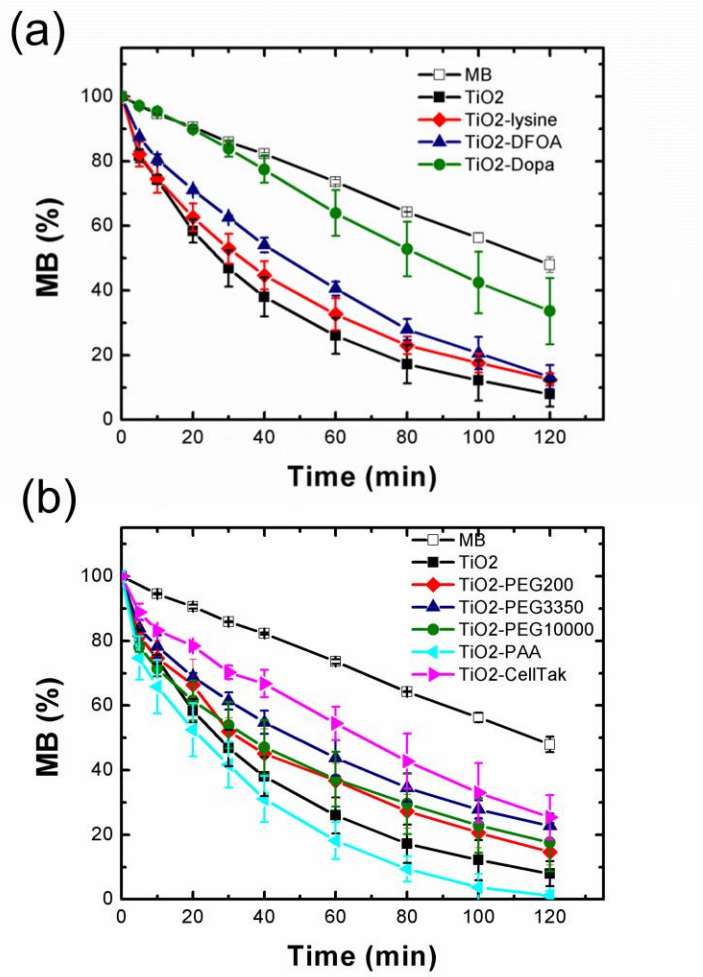

Fig. 7: Influence of the coating on the photo-catalytic activity. Degradation of MB under UV-vis irradiation with TiO_2 NPs (50 µg.mL^{-1}) coated with (a) biomolecules and (b) biopolymers. MB (%) = $((A_{665nm,\,t} - A_{665nm,t0})/A_{665nm,t0})$x100. Error bars determined from duplicate experiments.

Concerning the increase of the photocatalytic activity observed with PAA, the proximity of the polymer energy levels [64] — with a HOMO (highest occupied molecular orbital) and LUMO (lower unoccupied molecular orbital) located respectively at -7.6 eV and -4.0 eV — and the valence (E_{vb}) /conduction (E_{cb}) bands of anatase TiO_2 (E_{vb} = -7.1 eV; E_{cb} = -3.95 eV) [65] could favor the formation of a type II heterojunction between the polymer and the nanoparticles. Recently, Liu et al. [66] reported a so-called "Lock-in Effect" in a heterojunction of a COOH conjugated polymer and TiO_2 exhibiting outstanding photocatalytic activity. These new electronic properties resulted from the interfacial interaction between the carboxyl (also present in PAA) and hydroxyl groups of TiO_2, improving drastically the electron-hole separation efficiency and the interface charge transfer ability.

4. Paint formulation with TiO_2 NPs coated with bio-inspired ligands.

Finally, paints were formulated with different photocatalytic TiO_2 nanocomposites chosen according to their stability and photocatalytic activity (Table 1). Based on these criteria, uncoated TiO_2 (control), TiO_2-Dopa (high colloidal stability, -215% decrease of the photocatalytic activity), TiO_2-PEG3350 (high colloidal stability, -80% decrease of the photocatalytic activity) and TiO_2-PAA (high colloidal stability, +20% increase of the photocatalytic activity) NPs were selected and incorporated in paints at a 3.5 wt% TiO_2 content. After deposition on Leneta substrates, the paints were aged for one year in the dark or under interior day light (Fig. 8a). Whereas the paints exhibits a stable bright white coloration, the TiO_2-Dopa formulated paint possesses a characteristic brown color due to LMCT band issued from the covalent binding between Dopa and Ti sites on the TiO_2 NPs surface. This paint progressively turned to white after ageing in day light. This change of color can be associated to the progressive photodegradation of the Dopa coating by TiO_2 as suggested by the photocatalytic activity of the NPs and reported in the literature.[62]

Chalking assays performed after one year of storage (Fig. 8b) showed a high amount of collected powder on the tape with the TiO_2-PAA nanocomposites formulated paint (quotation of 5 and 4 after ageing in the dark and day light, respectively). This observation lets suggest a more intense degradation of the mechanical strength of the paint with this coating. Hence, it comes to confirm the enhanced photocatalytic activity exhibited by these NPs (+20%) compared to the original TiO_2 nanopowder. A decrease of the TiO_2 NP content by 20% could eventually be applied during the formulation to reduce the paint degradation and observe a comparable photocatalytic effect of the paint. The quotation of the TiO_2-Dopa paint after ageing in day light (quotation of 4) strongly increased compared to the aged in the dark and the TiO_2 control ones (quotations of 2), which could be the direct consequence of the degradation of the coating under irradiation as mentioned above. Among the three selected coatings, PEG3350 is the most promising one since the formulated paint appeared to be the most stable after ageing. This polymer is also relatively inexpensive and the NPs easy to prepare under mild conditions (e.g., without use of toxic solvents).

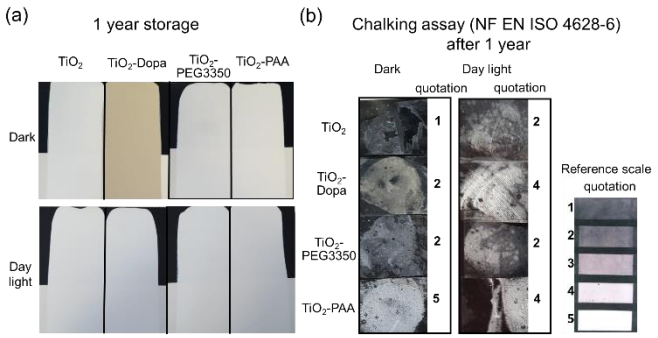

Fig. 8:(a) photographies of paints deposited on Leneta substrats after storage in dark and exposed to day light.and (b) chalking assay after storage for one year in dark or under interior day light of paints formulated with photocatalytic TiO_2 NPs uncoated or coated with Dopa, PEG3350 and PAA.

Conclusions

We successfully modified the surface of a commercial photocatalytic TiO_2 nanopowder with bio-inspired ligands of different chemical nature (molecules and polymers) for its application in self-cleaning paint. The coating strategy relied on the electrostatic stabilization in aqueous media with a pyrophosphate buffer (acid or basic conditions) followed by the addition of the ligand providing an extra steric stability compared to the initial particles.

The grafting and quantification of the ligand on the surface were confirmed by FTIR spectroscopy and TGA analysis performed on the nanocomposites. The grafting mode of several ligands was investigated by XPS and showed that the binding resulted from a combination of covalent and electrostatic interactions depending on the ligand chemical nature and architecture. These nanocomposites exhibit variable photocatalytic activities based on the degradation of MB under UV-vis irradiation, meeting our initial objective toward the safer-by-design development of a self-cleaning paint. As most of the ligands decreased more or less strongly the photocatalytic activity of the TiO_2 NPs, the nanocomposites should induce fewer damages to mechanical strength of the paint once incorporated in the paints while keeping the self-cleaning property. Only the coating with PAA presented an increase of the photocatalytic activity. With this feature, fewer particles in number would be necessary in the paint formulation for observing the same self-cleaning effect, and concomitantly, a lower amount of NPs would be released by mechanical stress, use or ageing over the paint life cycle. In order to improve the performance of the nanocomposites, the influence of the coating rate (thickness of the coating) on the photocatalytic properties, its resistance over several irradiation cycles and ageing would need to be investigated. The performance of these safer-by-design photocatalytic paints during their life cycle (photocatalytic efficiency, NPs emission during use, abrasion and incineration,

NPs toxicity and genotoxicity) should be further analyzed to evaluate their environmental benefits. Actually, the NPs and VOCs released during the use, weathering and mechanical solicitation of the formulated paints have been already further investigated and will be published in a separate paper.[20] It confirms the interest of our nanocomposites and our safer-by-design approach.

Conflicts of interest

There are no conflicts to declare.

Acknowledgements

The authors acknowledge Stéphane Ménage and Aurélien Deniaud for interesting discussions. This work is a contribution to the LABEX SERENADE (n° ANR-11-LABX-0064) funded by the "Investissements d'Avenir" French Government program of the French National Research Agency (ANR) through the A*MIDEX project (N° ANR-11-IDEX-0001-02). This research is part of the LabEx ARCANE and CBH-EURGS (grant ANR-17-EURE-0003). JL and AR were supported by the SafeTiPaint project granted by the LabEx SERENADE. The NanoZS were funded by the EQUIPEX NanoID (grant ANR-10-EQPX-39-01).

Abbreviation

TiO_2 NPs: Titanium dioxide nanoparticles; DFOA: Deferoxamine; Dopa: Dopamine; PAA: Poly-acrylic acid; PEG: Polyethylene glycol; MB: Methylene blue; H_2Pyro and NaPyro: acidic ($Na_2H_2P_2O_7$, pH 4.5) and alkaline forms ($Na_4P_2O_7$, pH 8.5) of pyrophosphate, respectively; FTIR: Fourrier-transformed infrared; SEM: Scanning electron micrography; EDX: Energy-dispersive X-ray spectroscopy.

References

1. J. Jeevanandam, A. Barhoum, Y. S. Chan, A. Dufresne and M. K. Danquah, Review on nanoparticles and nanostructured materials: history, sources, toxicity and regulations, *Beilstein J. Nanotechnol.*, 2018, **9**, 1050-1074.
2. M. Usman, M. Farooq, A. Wakeel, A. Nawaz, S. A. Cheema, H. u. Rehman, I. Ashraf and M. Sanaullah, Nanotechnology in agriculture: Current status, challenges and future opportunities, *Sci. Tot. Environ.*, 2020, **721**, 137778.
3. S. D. F. Mihindukulasuriya and L. T. Lim, Nanotechnology development in food packaging: A review, *Trends Food Sci. Technol.*, 2014, **40**, 149-167.
4. L. Kaounides, H. Yu and T. Harper, Nanotechnology innovation and applications in textiles industry: current markets and future growth trends, *Mater. Technol.*, 2007, **22**, 209-237.
5. V. Kostopoulos, A. Masouras, A. Baltopoulos, A. Vavouliotis, G. Sotiriadis and L. Pambaguian, A critical review of nanotechnologies for composite aerospace structures, *CEAS Space J.*, 2017, **9**, 35-57.
6. O. M. Koo, I. Rubinstein and H. Onyuksel, Role of nanotechnology in targeted drug delivery and imaging: a concise review, *Nanomedicine*, 2005, **1**, 193-212.
7. M. T. Alsaba, M. F. Al Dushaishi and A. K. Abbas, A comprehensive review of nanoparticles applications in the oil and gas industry, *J. Petrol. Explor. Prod. Technol.*, 2020, **10**, 1389-1399.
8. The Nanodatabase, http://www.nanodb.dk .
9. S. Foss Hansen, L. R. Heggelund, P. Revilla Besora, A. Mackevica, A. Boldrin and A. Baun, Nanoproducts – what is actually available to European consumers?, *Environ. Sci. Nano*, 2016, **3**, 169-180.
10. J.-P. Kaiser, S. Zuin and P. Wick, Is nanotechnology revolutionizing the paint and lacquer industry? A critical opinion, *Sci. Tot. Environ.*, 2013, **442**, 282-289.
11. A. Fujishima, T. N. Rao and D. A. Tryk, Titanium dioxide photocatalysis, *J. Photochem. Photobiol. C*, 2000, **1**, 1-21.
12. X. Chen and S. S. Mao, Titanium Dioxide Nanomaterials: Synthesis, Properties, Modifications, and Applications, *Chem. Rev.*, 2007, **107**, 2891-2959.
13. A. Gandolfo, L. Rouyer, H. Wortham and S. Gligorovski, The influence of wall temperature on NO_2 removal and HONO levels released by indoor photocatalytic paints, *Appl. Catal. B*, 2017, **209**, 429-436.
14. B. Fiorentino, L. Golanski, A. Guiot, J. F. Damlencourt and D. Boutry, Influence of paints formulations on nanoparticles release during their life cycle, *J. Nanopart. Res.*, 2015, **17**.
15. D. Truffier-Boutry, B. Fiorentino, V. Bartolomei, R. Soulas, O. Sicardy, A. Benayad, J. F. Damlencourt, B. Pepin-Donat, C. Lombard, A. Gandolfo, H. Wortham, G. Brochard, A. Audemard, L. Porcar, G. Gebel and S. Gligorovski, Characterization of photocatalytic paints: a relationship between the photocatalytic properties - release of nanoparticles and volatile organic compounds, *Environ. Sci. Nano*, 2017, **4**, 1998-2009.
16. A. T. Saber, K. A. Jensen, N. R. Jacobsen, R. Birkedal, L. Mikkelsen, P. Moller, S. Loft, H. Wallin and U. Vogel, Inflammatory and genotoxic effects of nanoparticles designed for inclusion in paints and lacquers, *Nanotoxicology*, 2012, **6**, 453-471.
17. S. Lin, T. Yu, Z. Yu, X. Hu and D. Yin, Nanomaterials safer-by-design: an environmental safety perspective, *Adv. Mater.*, 2018, **30**, 1705691.
18. J. Y. Bottero, J. Rose, C. de Garidel, A. Masion, T. Deutsch, G. Brochard, M. Carriere, N. Gontard, H. Wortham, T. Rabilloud, B. Salles, M. Dubosson, B. Cathala, D. Boutry, A. Ereskovsky, C. Auplat, L. Charlet, T. Heulin, E. Frejafon and S. Lanone, SERENADE: safer and ecodesign research and education applied to nanomaterial development, the new generation of materials safer by design, *Environ. Sci-Nano*, 2017, **4**, 526-538.
19. H. Park, Y. Park, W. Kim and W. Choi, Surface modification of TiO2 photocatalyst for environmental applications, *J. Photochem. Photobiol. C*, 2013, **15**, 1-20.
20. A. Rosset, V. Bartolomei, J. Laisney, N. Shandilya, H. Voisin, J. Morin, I. Michaud-Soret, I. Capron, H. Wortham, G. Brochard, V. Bergé, M. Carriere, F. Dussert, O. Le Bihan, C. Dutouquet, D. Truffier-Boutry, S. Clavaguera, S. Artous, Towards the

development of Safer by Design TiO_2-based photocatalytic paint: impacts and performances, *Environ. Sci.: Nano*, 2020, Submitted.

21. I. A. Jankovic, Z. V. Saponjic, E. S. Dzunuzovic and J. M. Nedeljkovic, New Hybrid Properties of TiO_2 Nanoparticles Surface Modified With Catecholate Type Ligands, *Nanoscale Res. Lett.*, 2010, **5**, 81-88.
22. J. Yu, W. Wei, M. S. Menyo, A. Masic, J. H. Waite and J. N. Israelachvili, Adhesion of Mussel Foot Protein-3 to TiO_2 Surfaces: the Effect of pH, *Biomacromolecules*, 2013, **14**, 1072-1077.
23. J. Manson, D. Kumar, B. J. Meenan and D. Dixon, Polyethylene glycol functionalized gold nanoparticles: the influence of capping density on stability in various media (vol 44, pg 99, 2011), *Gold Bull.*, 2011, **44**, 195-196.
24. J. B. Luo, S. X. Qiu, X. Y. Zhou, R. H. Lai, P. J. Dong and X. Y. Xie, In situ grafting polyethylene glycol chains onto amorphous calcium phosphate nanoparticles to improve the storage stability and organic solvent redispersibility, *Colloid Surf. A*, 2014, **444**, 81-88.
25. E. Harrison, J. R. Nicol, M. Macias-Montero, G. A. Burke, J. A. Coulter, B. J. Meenan and D. Dixon, A comparison of gold nanoparticle surface co-functionalization approaches using Polyethylene Glycol (PEG) and the effect on stability, non-specific protein adsorption and internalization, *Mat. Sci. Eng. C-Mater*, 2016, **62**, 710-718.
26. J. Eisenlauer, E. Killmann and M. Korn, Stability of Colloidal Silica (Aerosil) Hydrosols .2. Influence of the Ph Value and the Adsorption of Polyethylene Glycols, *J. Colloid. Interf. Sci.*, 1980, **74**, 120-135.
27. S. C. Liufu, H. N. Xiao, Y. P. Li and Z. R. Hu, Polyethylene glycol adsorption behavior on nanoparticulate TiO_2 and its stability in aqueous dispersions, *J. Inorg. Mater.*, 2005, **20**, 310-316.
28. H. B. Na, G. Palui, J. T. Rosenberg, X. Ji, S. C. Grant and H. Mattoussi, Multidentate Catechol-Based Polyethylene Glycol Oligomers Provide Enhanced Stability and Biocompatibility to Iron Oxide Nanoparticies, *Acs Nano*, 2012, **6**, 389-399.
29. M. F. Tai, C. W. Lai and S. B. A. Hamid, Facile Synthesis Polyethylene Glycol Coated Magnetite Nanoparticles for High Colloidal Stability, *J. Nanomater.*, 2016, DOI: 10.1155/2016/8612505.
30. T. J. Deming, Mussel byssus and biomolecular materials, *Curr. Opin. Chem. Biol.*, 1999, **3**, 100-105.
31. G. P. Maier and A. Butler, Siderophores and mussel foot proteins: the role of catechol, cations, and metal coordination in surface adhesion, *J. Biol. Inorg. Chem.*, 2017, **22**, 739-749.
32. G. P. Maier, M. V. Rapp, J. H. Waite, J. N. Israelachvili and A. Butler, BIOLOGICAL ADHESIVES. Adaptive synergy between catechol and lysine promotes wet adhesion by surface salt displacement, *Science*, 2015, **349**, 628-632.
33. J. H. Waite, Mussel glue fromMytilus californianus Conrad: a comparative study, *J. Comp. Physiol. B*, 1986, **156**, 491-496.
34. S. V. Sokolov, K. Tschulik, C. Batchelor-McAuley, K. Jurkschat and R. G. Compton, Reversible or Not? Distinguishing Agglomeration and Aggregation at the Nanoscale, *Anal. Chem.*, 2015, **87**, 10033-10039.
35. B. Derjaguin and L. Landau, Theory of the stability of strongly charged lyophobic sols and of the adhesion of strongly charged particles in solutions of electrolytes, *Prog. Surf. Sci.*, 1993, **43**, 30-59.
36. M. Wiśniewska, T. Urban, E. Grządka, V. I. Zarko and V. M. Gun'ko, Comparison of adsorption affinity of polyacrylic acid for surfaces of mixed silica-alumina, *Colloid. Polym. Sci.*, 2014, **292**, 699-705.
37. W. Wei, J. Yu, C. Broomell, J. N. Israelachvili and J. H. Waite, Hydrophobic Enhancement of Dopa-Mediated Adhesion in a Mussel Foot Protein, *J. Am. Chem. Soc.*, 2013, **135**, 377-383.
38. I. A. Jankovic, Z. V. Saponjic, M. I. Comor and J. M. Nedeljlkovic, Surface Modification of Colloidal TiO_2 Nanoparticles with Bidentate Benzene Derivatives, *J. Phys. Chem. C*, 2009, **113**, 12645-12652.
39. S. S. Mali, C. A. Betty, P. N. Bhosale and P. S. Patil, Synthesis, Characterization of Hydrothermally Grown MWCNT–TiO2Photoelectrodes and Their Visible Light Absorption Properties, *ECS J. Solid State Sci. Technol.*, 2012, **1**, M15-M23.
40. V. A. Tran, T. T. Truong, T. A. P. Phan, T. N. Nguyen, T. V. Huynh, A. Agresti, S. Pescetelli, T. K. Le, A. Di Carlo, T. Lund, S.-N. Le and P. T. Nguyen, Application of nitrogen-doped TiO_2 nano-tubes in dye-sensitized solar cells, *Appl. Surf. Sci.*, 2017, **399**, 515-522.
41. , High Resolution XPS of Organic Polymers: The Scienta ESCA300 Database (Beamson, G.; Briggs, D.), *J. Chem. Educ.*, 1993, **70**, A25.
42. Q. Wang, N. Plylahan, M. V. Shelke, R. R. Devarapalli, M. Li, P. Subramanian, T. Djenizian, R. Boukherroub and S. Szunerits, Nanodiamond particles/reduced graphene oxide composites as efficient supercapacitor electrodes, *Carbon*, 2014, **68**, 175-184.
43. F. Zhang, J. Tang, Z. Wang and L.-C. Qin, Graphene–carbon nanotube composite aerogel for selective detection of uric acid, *Chem. Phys. Lett.*, 2013, **590**, 121-125.
44. S. Liu, J. Sun and Z. Huang, Carbon spheres/activated carbon composite materials with high Cr(VI) adsorption capacity prepared by a hydrothermal method, *J. Hazard. Mater.*, 2010, **173**, 377-383.
45. W. H. Lee, S. J. Kim, W. J. Lee, J. G. Lee, R. C. Haddon and P. J. Reucroft, X-ray photoelectron spectroscopic studies of surface modified single-walled carbon nanotube material, *Appl. Surf. Sci.*, 2001, **181**, 121-127.
46. T. I. T. Okpalugo, P. Papakonstantinou, H. Murphy, J. McLaughlin and N. M. D. Brown, High resolution XPS characterization of chemical functionalised MWCNTs and SWCNTs, *Carbon*, 2005, **43**, 153-161.
47. S. Pan, X. Liu, M. Guo, S. f. Yu, H. Huang, H. Fan and G. Li, Engineering the intermediate band states in amorphous Ti^{3+}-doped TiO_2 for hybrid dye-sensitized solar cell applications, *J. Mater. Chem. A*, 2015, **3**, 11437-11443.
48. M. C. Biesinger, L. W. M. Lau, A. R. Gerson and R. S. C. Smart, Resolving surface chemical states in XPS analysis of first row transition metals, oxides and hydroxides: Sc, Ti, V, Cu and Zn, *Appl. Surf. Sci.*, 2010, **257**, 887-898.
49. M. G. Faba, D. Gonbeau and G. Pfister-Guillouzo, Core and valence spectra of titanium dichalcogenides TiX_2 (where X is

O, S). Experimental and theoretical studies, *J. Electron Spectros. Relat. Phenomena*, 1995, **73**, 65-80.
50. D. Zhao, C. Chen, Y. Wang, H. Ji, W. Ma, L. Zang and J. Zhao, Surface Modification of TiO_2 by Phosphate: Effect on Photocatalytic Activity and Mechanism Implication, *J. Phys. Chem. C*, 2008, **112**, 5993-6001.
51. K. Raj, R. Shanmugam, R. Mahalakshmi and B. Viswanathan, XPS and IR spectral studies on the structure of phosphate and sulphate modified titania–a combined DFT and experimental study, 2010.
52. P. Georgios and S. M. Wolfgang, X-Ray Photoelectron Spectroscopy of Anatase-TiO_2 Coated Carbon Nanotubes, *Solid State Phenomena*, 2010, **162**, 163-177.
53. X. Bai, T. Li, Y.-X. Qi, Y.-X. Wang, L.-W. Yin, H. Li, N. Lun and Y.-J. Bai, One-step fabricating nitrogen-doped TiO_2 nanoparticles coated with carbon to achieve excellent high-rate lithium storage performance, *Electrochim. Acta*, 2016, **187**, 389-396.
54. H. Ming, J. Ming, X. Li, Q. Zhou, H. Wang, L. Jin, Y. Fu, J. Adkins and J. Zheng, Hierarchical $Li_4Ti_5O_{12}$ particles co-modified with C&N towards enhanced performance in lithium-ion battery applications, *Electrochim. Acta*, 2014, **116**, 224-229.
55. R. Gouttebaron, D. Cornelissen, R. Snyders, J. P. Dauchot, M. Wautelet and M. Hecq, XPS study of TiO_x thin films prepared by d.c. magnetron sputtering in Ar–O2 gas mixtures, *Surf. Interface Anal.*, 2000, **30**, 527-530.
56. N. C. Saha and H. G. Tompkins, Titanium nitride oxidation chemistry: An x-ray photoelectron spectroscopy study, *J. Appl. Phys.*, 1992, **72**, 3072-3079.
57. L. Avalle, E. Santos, E. Leiva and V. A. Macagno, Characterization of TiO_2 films modified by platinum doping, *Thin Solid Films*, 1992, **219**, 7-17.
58. B. Xin, P. Wang, D. Ding, J. Liu, Z. Ren and H. Fu, Effect of surface species on Cu-TiO_2 photocatalytic activity, *Appl. Surf. Sci.*, 2008, **254**, 2569-2574.
59. H. Liu, J. Liu, W. Song, F. Wang and Y. Song, Li_xCo_3-xO_4 solid solution nanocrystals supported on carbon black as a superior electrocatalyst for oxygen reduction reaction, *Mater. Lett.*, 2015, **139**, 447-450.
60. I. A. Jankovic, Z. V. Saponjic, M. I. Comor and J. M. Nedeljkovic, Surface modification of colloidal TiO_2 nanoparticles with bidentate benzene derivatives, *J. Phys. Chem. C*, 2009, **113**, 12645-12652.
61. Nasikhudin, M. Diantoro, A. Kusumaatmaja and K. Triyana, Study on Photocatalytic Properties of TiO_2 Nanoparticle in various pH condition, *J. Phys. Conf. Ser.*, 2018, **1011**, 012069.
62. A. L. Chibac, T. Buruiana, V. Melinte and E. C. Buruiana, Photocatalysis applications of some hybrid polymeric composites incorporating TiO_2 nanoparticles and their combinations with SiO_2/Fe_2O_3, *Beilstein J. Nanotechnol.*, 2017, **8**, 272-286.
63. Y. Nam, J. H. Lim, K. C. Ko and J. Y. Lee, Photocatalytic activity of TiO2 nanoparticles: a theoretical aspect, *J. Mater. Chem. A*, 2019, **7**, 13833-13859.
64. Y. Zhu, A. Apostoluk, P. Gautier, A. Valette, L. Omar, T. Cornier, J. M. Bluet, K. Masenelli-Varlot, S. Daniele and B. Masenelli, Intense visible emission from ZnO/PAAX (X = H or Na) nanocomposite synthesized via a simple and scalable sol-gel method, *Sci. Rep.*, 2016, **6**, 23557.
65. C. Maheu, L. Cardenas, E. Puzenat, P. Afanasiev and C. Geantet, UPS and UV spectroscopies combined to position the energy levels of TiO_2 anatase and rutile nanopowders, *Phys. Chem. Chem. Phys.*, 2018, **20**, 25629-25637.
66. L. Liu, W. Jiang, X. Song, Q. Duan and E. Zhu, A novel Strategy of Lock-in Effect between Conjugated Polymer and TiO_2 towards Dramatic Enhancement of Photocatalytic Activity under Visible Light, *Sci. Rep.*, 2020, **10**, 6513.

